

















RESEARCH ARTICLE | DECEMBER 07 2023

Electronic band structure of superconducting KTaO_3 (111) interfaces

Srijani Mallik ; Borge Göbel ; Hugo Witt ; Luis M. Vicente-Arche ; Sara Varotto; Julien Bréhin ; Gerbold Ménard ; Guilhem Saiz; Dyhia Tamsaout; Andrés Felipe Santander-Syro ; Franck Fortuna ; François Bertran ; Patrick Le Fèvre ; Julien Rault ; Isabella Boventer ; Ingrid Mertig ; Agnès Barthélémy ; Nicolas Bergeal ; Annika Johansson ; Manuel Bibes 



APL Mater. 11, 121108 (2023)

<https://doi.org/10.1063/5.0169750>



CrossMark



APL Quantum
First Articles Online
No Article Processing Charges for Submissions
Through December 31, 2024
[Read Now](#)



Electronic band structure of superconducting KTaO_3 (111) interfaces

Cite as: APL Mater. 11, 121108 (2023); doi: 10.1063/5.0169750

Submitted: 28 July 2023 • Accepted: 13 November 2023 •

Published Online: 7 December 2023



View Online



Export Citation



CrossMark

Srijani Mallik,^{1,a)} Börge Göbel,^{2,b)} Hugo Witt,^{1,3} Luis M. Vicente-Arche,¹ Sara Varotto,¹ Julien Bréhin,¹ Gerbold Ménard,³ Guilhem Saiz,³ Dyhia Tamsaout,¹ Andrés Felipe Santander-Syro,⁴ Franck Fortuna,⁴ François Bertran,⁵ Patrick Le Fèvre,⁵ Julien Rault,⁵ Isabella Boverter,¹ Ingrid Mertig,² Agnès Barthélémy,¹ Nicolas Bergeal,³ Annika Johansson,^{6,c)} and Manuel Bibes^{1,d)}

AFFILIATIONS

¹Unité Mixte de Physique, CNRS, Thales, Université Paris-Saclay, 91767 Palaiseau, France

²Institut für Physik, Martin-Luther-Universität Halle-Wittenberg, 06099 Halle, Germany

³Laboratoire de Physique et d'Etude des Matériaux, ESPCI Paris, Université PSL, CNRS, 75005 Paris, France

⁴Institut des Sciences Moléculaires d'Orsay, CNRS, Université Paris-Saclay, 91405 Orsay, France

⁵SOLEIL Synchrotron, L'Orme des Merisiers, Départementale 128, F-91190 Saint-Aubin, France

⁶Max Planck Institute of Microstructure Physics, Weinberg 2, 06120 Halle, Germany

^{a)}Author to whom correspondence should be addressed: srijani.mallik@cnrs-thales.fr

^{b)}Electronic mail: boerge.goebel@physik.uni-halle.de

^{c)}Electronic mail: annika.johansson@mpi-halle.mpg.de

^{d)}Electronic mail: manuel.bibes@cnrs-thales.fr

ABSTRACT

Two-dimensional electron gases (2DEGs) based on KTaO_3 are emerging as a promising platform for spin-orbitronics due to their high Rashba spin-orbit coupling (SOC) and gate-voltage tunability. The recent discovery of a superconducting state in KTaO_3 2DEGs now expands their potential towards topological superconductivity. Although the band structure of KTaO_3 surfaces of various crystallographic orientations has already been mapped using angle-resolved photoemission spectroscopy (ARPES), this is not the case for superconducting KTaO_3 2DEGs. Here, we reveal the electronic structure of superconducting 2DEGs based on KTaO_3 (111) single crystals through ARPES measurements. We fit the data with a tight-binding model and compute the associated spin textures to bring insight into the SOC-driven physics of this fascinating system.

© 2023 Author(s). All article content, except where otherwise noted, is licensed under a Creative Commons Attribution (CC BY) license (<http://creativecommons.org/licenses/by/4.0/>). <https://doi.org/10.1063/5.0169750>

I. INTRODUCTION

Oxide interfaces can harbor exotic phases of condensed matter, often absent in the interface constituents of their bulk form.^{1,2} A paradigmatic example is the SrTiO_3 (STO) two-dimensional electron gas (2DEG) that forms when STO is interfaced with epitaxial oxides, such as LaAlO_3 (LAO),³ or through local redox processes occurring at the interface when STO is covered with a reactive metal, such as Al or Ta.^{4–6} While some properties of STO 2DEGs can be found in bulk STO, including high mobility transport⁷ and low temperature superconductivity,⁸ these are often superior or of different nature in STO 2DEGs. For instance, mobilities exceeding 10^5 cm^2

$\text{V}^{-1} \text{ s}^{-1}$ have been reported in STO-based 2DEGs,⁹ while the record value for bulk STO is $\sim 10^4 \text{ cm}^2 \text{ V}^{-1} \text{ s}^{-1}$. Another instance is superconductivity in STO 2DEGs is two-dimensional¹⁰ and highly tunable by electrostatic gating.¹¹ Moreover, 2DEGs also display unique features, such as Rashba spin-orbit coupling (SOC),¹² which only arises in environments with broken inversion symmetry (e.g., surfaces or interfaces), and shows intrinsic signatures of two-dimensional transport, such as the quantum Hall effect.¹³

Key insight into the physics of STO 2DEGs was gained through angle-resolved photoemission spectroscopy (ARPES) by mapping their electronic structure. Such measurements revealed band splittings and sub-bands arising from quantum confinement,^{14–17} which

are absent in the bulk.¹⁸ Most ARPES results have been collected on (001)-oriented STO 2DEGs and have shown the coexistence of bands having a d_{xy} orbital character with a low effective mass and bands having a $d_{xz/yz}$ character with a higher effective mass. Orbital mixing due to the reduced symmetry produces avoided crossings where SOC-related effects are enhanced.¹⁷ Such studies dramatically advanced the understanding of the superconducting phase diagram (with heavier bands playing a key role) and of spin–charge interconversion phenomena driven by the Rashba SOC.^{17,19–22} The electronic structure of STO 2DEGs grown along other crystal orientations, namely (110) and (111), has also been mapped by ARPES.^{23,24} These experiments helped to understand the differences in their physical responses, notably regarding the dependence of superconductivity on the Fermi energy. For 2DEGs oriented along (110) and (111) directions, this dependence is much less pronounced due to their reduced orbital splitting (see, e.g., Refs. 25 and 26).

Similar to STO, KTaO_3 (KTO) is a quantum paraelectric that, in the bulk, becomes metallic upon minute electron doping.^{7,27} This prompted the exploration of KTO interfaces a few years after the discovery of STO 2DEGs.^{28–31} Aside from measurements on ionic-liquid gated crystals showing an ultralow critical temperature T_c of 40 mK,³² initially no superconductivity was found in KTO 2DEGs, consistent with the absence of superconducting properties in bulk KTO.³³ At first, efforts on KTO 2DEGs were concentrated on the (001) orientation, and one notable finding was the presence of a large Rashba SOC through weak antilocalization or spin–charge interconversion experiments,³⁴ where the Rashba coefficient was found to be 5–10 times larger than in STO, as expected from the heavier mass of Ta compared to Ti. The sizable band splitting induced by Rashba SOC was sufficiently large to be directly imaged by ARPES,³⁵ which also revealed bands with well-defined orbital character, akin to the situation in STO 2DEGs.

In this context, the discovery of superconductivity with a T_c up to 2.2 K in (111)-oriented KTO 2DEGs came as a big surprise.³⁶ This finding was soon confirmed by different groups; see, e.g., Refs. 37–39. Superconductivity was also found up to about 1 K in (110)-oriented KTO 2DEGs.⁴⁰ Until now, the reasons for this huge orientational dependence—at odds with the situation in STO 2DEGs—have not been clarified, even if some theoretical proposals have recently emerged discussing the role of electron–phonon coupling or the Rashba SOC in driving the superconductivity.^{41–43} To resolve this conundrum, high quality ARPES measurements are needed to precisely map and understand the electronic structure of superconducting KTO 2DEGs. A few years before the discovery of superconductivity in KTO (111), two studies reported the band structure of KTO (111) surfaces using ARPES.^{44,45} The band structure of KTO (110) 2DEGs was also reported not long ago.⁴⁶ Yet, whether these samples were superconducting or not remains unknown. Recently, Chen *et al.* reported ARPES data for KTO (001), superconducting KTO (110) and (111), measured using soft x-rays with 1000 eV photon energy. However, due to this high photon energy, it was not possible to resolve the exact band structure near the Fermi energy.⁴⁷

In this paper, we report the electronic structure of KTO (111) 2DEGs measured by ARPES with high energy resolution using a photon energy of 31 eV. The samples are prepared by depositing a few Å of Eu, triggering a redox reaction to form a 2DEG. They are superconducting with an anisotropic T_c of 0.6 and 0.8 K, depending

on the direction along which the current is applied. The dispersion curves and Fermi surfaces obtained by ARPES were fitted with four spin-resolved band pairs below the Fermi energy. We calculate the band-resolved spin textures as a function of energy and discuss the results in light of future spin–charge interconversion experiments and the origin of superconductivity in this system.

II. METHODS

A. Sample preparation

Single crystalline KTO (111) substrates from MTI Corporation were pre-annealed at 300 °C for 2 h in an ultra-high vacuum inside a molecular beam epitaxy (MBE) chamber. We grew 3 Å of Eu at 300 °C using a Knudsen cell heated to 500 °C at a growth rate of 0.043 Å s^{−1} and a deposition pressure of 1.2×10^{-9} mbar. Subsequently, the sample was transferred *in situ* to the ARPES chamber.

For *ex situ* transport measurement, another sample with 3 Å Eu was prepared in the exact same deposition conditions. In order to protect the 2DEG at the Eu/KTO (111) interface from oxidation from the air, we capped the sample *in situ* with 2.1 nm of Al grown at room temperature using a Knudsen cell heated to 1000 °C at a growth rate of 0.092 Å s^{−1}. Thus, the Al overlayer was spontaneously and completely oxidized into AlO_x when exposed to the air prior to the transport measurements. Both samples were grown on two pieces cleaved from the same KTO (111) substrate.

B. Angular resolved photoemission spectroscopy

High-resolution angular resolved photoemission spectroscopy (ARPES) measurements were performed at the Cassiopée beamline of Synchrotron SOLEIL (France). This beamline is equipped with a Scienta R4000 hemispherical electron energy analyzer. All the measurements were performed at 15 K (sample space cooled by liquid He) in order to minimize the thermal broadening of the spectral lines. The energy and angular resolution were 15 meV and $<0.25^\circ$, respectively. The data presented in the manuscript were collected with linearly horizontally (LH) polarized photons with a photon energy of 31 eV. The collected data were normalized by taking the second derivative of the intensity background of the electron analyzer and smoothed using an averaging filter.

C. Tight-binding model

Our tight-binding (TB) model considers 36 bands (18 band pairs). One unit cell considers three of each of the $5d$ Ta t_{2g} orbitals (d_{xy} , d_{xz} , and d_{yz}) giving rise to the basis

$$\begin{aligned} & \{ |d_{xy1\uparrow}\rangle, |d_{xy1\downarrow}\rangle, |d_{yz1\uparrow}\rangle, |d_{yz1\downarrow}\rangle, |d_{zx1\uparrow}\rangle, |d_{zx1\downarrow}\rangle, \\ & |d_{xy2\uparrow}\rangle, |d_{xy2\downarrow}\rangle, |d_{yz2\uparrow}\rangle, |d_{yz2\downarrow}\rangle, |d_{zx2\uparrow}\rangle, |d_{zx2\downarrow}\rangle, \\ & |d_{xy3\uparrow}\rangle, |d_{xy3\downarrow}\rangle, |d_{yz3\uparrow}\rangle, |d_{yz3\downarrow}\rangle, |d_{zx3\uparrow}\rangle, |d_{zx3\downarrow}\rangle \}. \end{aligned} \quad (1)$$

We add another copy with different parameters to reproduce the sub-bands arising due to the quantum confinement of electrons near the surface. We diagonalize the tight-binding Hamiltonian

$$H = H_{\text{hop}} + H_{\text{SOC}} + H_{\text{mix}} \quad (2)$$

to describe the electron gas that is confined at the interface of KTO (111) with a lattice constant $a = 4.0$ Å formed by the Ta atoms.

For the hopping term, we consider

$$H_{\text{hop}} = \begin{pmatrix} \Delta\varepsilon & 0 & 0 & h_{\pi}^{-x} + h_{\pi}^{-y} + h_{\delta}^{-z} & 0 & 0 & 0 & 0 & 0 \\ 0 & \Delta\varepsilon & 0 & 0 & h_{\delta}^{-x} + h_{\pi}^{-y} + h_{\pi}^{-z} & 0 & 0 & 0 & 0 \\ 0 & 0 & \Delta\varepsilon & 0 & 0 & h_{\pi}^{-x} + h_{\delta}^{-y} + h_{\pi}^{-z} & 0 & 0 & 0 \\ h_{\pi}^x + h_{\pi}^y + h_{\delta}^z & 0 & 0 & \Delta\varepsilon & 0 & 0 & h_{\pi}^{-x} + h_{\pi}^{-y} + h_{\delta}^{-z} & 0 & 0 \\ 0 & h_{\delta}^x + h_{\pi}^y + h_{\pi}^z & 0 & 0 & \Delta\varepsilon & 0 & 0 & h_{\delta}^{-x} + h_{\pi}^{-y} + h_{\pi}^{-z} & 0 \\ 0 & 0 & h_{\pi}^x + h_{\delta}^y + h_{\pi}^z & 0 & 0 & \Delta\varepsilon & 0 & 0 & h_{\pi}^{-x} + h_{\delta}^{-y} + h_{\pi}^{-z} \\ 0 & 0 & 0 & h_{\pi}^x + h_{\pi}^y + h_{\delta}^z & 0 & 0 & \Delta\varepsilon & 0 & 0 \\ 0 & 0 & 0 & 0 & h_{\delta}^x + h_{\pi}^y + h_{\pi}^z & 0 & 0 & \Delta\varepsilon & 0 \\ 0 & 0 & 0 & 0 & 0 & h_{\pi}^x + h_{\delta}^y + h_{\pi}^z & 0 & 0 & \Delta\varepsilon \end{pmatrix} \otimes \begin{pmatrix} 1 & 0 \\ 0 & 1 \end{pmatrix} \quad (3)$$

with $h_{\alpha}^j = t_{\alpha} e^{iak_j}$ indicating the nearest-neighbor $\alpha = \{\pi, \delta\}$ hopping of the $\{d_{xy}, d_{yz}, d_{zx}\}$ orbitals along $\{x, y, z\}$ according to the Slater–Koster rules. The linearly independent hopping amplitudes are $t_{\pi} = -0.65$ eV and $t_{\delta} = -0.05$ eV. Note that the σ hopping is not relevant for nearest-neighbor hoppings considering only the t_{2g} orbitals. The onsite energies are $\Delta\varepsilon = 1.946$ eV (and $\Delta\varepsilon = 2.011$ eV for the sub-bands), causing a shift of the bands in energy.

The gradient potential at the interface displaces the oxygen's p orbitals away from the bond connecting two neighboring Ta atoms. Hopping terms that were forbidden in bulk are now allowed by the Slater–Koster rules. By analogy with KTO (001) 2DEGs, discussed in Ref. 35, hopping between two neighboring Ta d orbitals, via an intermediate hopping to an oxygen p orbital, causes an effective hopping network. The hopping is asymmetric and gives rise to orbital mixing terms,

$$H_{\text{mix}} = g \begin{pmatrix} 0 & 0 & 0 & 0 & e^{-iak_z} - e^{-iak_x} & e^{-iak_z} - e^{-iak_y} & 0 & 0 & 0 \\ 0 & 0 & 0 & e^{-iak_x} - e^{-iak_z} & 0 & e^{-iak_x} - e^{-iak_y} & 0 & 0 & 0 \\ 0 & 0 & 0 & e^{-iak_y} - e^{-iak_z} & e^{-iak_y} - e^{-iak_x} & 0 & 0 & 0 & 0 \\ 0 & e^{iak_x} - e^{iak_z} & e^{iak_y} - e^{iak_z} & 0 & 0 & 0 & 0 & e^{-iak_z} - e^{-iak_x} & e^{-iak_z} - e^{-iak_y} \\ e^{iak_z} - e^{iak_x} & 0 & e^{iak_y} - e^{iak_x} & 0 & 0 & 0 & e^{-iak_x} - e^{-iak_z} & 0 & e^{-iak_x} - e^{-iak_y} \\ e^{iak_z} - e^{iak_y} & e^{iak_x} - e^{iak_y} & 0 & 0 & 0 & 0 & e^{-iak_y} - e^{-iak_z} & e^{-iak_y} - e^{-iak_x} & 0 \\ 0 & 0 & 0 & 0 & e^{iak_x} - e^{iak_z} & e^{iak_y} - e^{iak_z} & 0 & 0 & 0 \\ 0 & 0 & 0 & e^{iak_z} - e^{iak_x} & 0 & e^{iak_y} - e^{iak_x} & 0 & 0 & 0 \\ 0 & 0 & 0 & e^{iak_z} - e^{iak_y} & e^{iak_x} - e^{iak_y} & 0 & 0 & 0 & 0 \end{pmatrix} \otimes \begin{pmatrix} 1 & 0 \\ 0 & 1 \end{pmatrix} \quad (4)$$

The amplitude is $g = 3$ meV (and $g = 1$ meV for the sub-bands).

H_{SOC} with $\lambda = 0.4$ eV describes the on-site spin-orbit coupling, which mixes the different spin orientations and orbitals. It is the same for each lattice site and reads

$$H_{\text{SOC}} = \frac{\lambda}{3} \begin{pmatrix} 0 & 0 & 0 & 1 & 0 & -i \\ 0 & 0 & -1 & 0 & -i & 0 \\ 0 & -1 & 0 & 0 & i & 0 \\ 1 & 0 & 0 & 0 & 0 & -i \\ 0 & i & -i & 0 & 0 & 0 \\ i & 0 & 0 & i & 0 & 0 \end{pmatrix} \quad (5)$$

in the basis $\{|d_{xy\uparrow}\rangle, |d_{xy\downarrow}\rangle, |d_{yz\uparrow}\rangle, |d_{yz\downarrow}\rangle, |d_{zx\uparrow}\rangle, |d_{zx\downarrow}\rangle\}$.

D. Transport measurements

The transport measurements were performed in DC with the current flowing along the $[\bar{1}\bar{1}0]$ and $[\bar{1}\bar{1}2]$ directions of the sample inside a dilution refrigerator with a base temperature of 25 mK. The sample holder is thermally decoupled from the mixing chamber plate to allow a continuous temperature sweep from 25 mK to 2 K.

III. RESULTS AND DISCUSSION

A. Structural and transport properties

Figure 1 exhibits the temperature dependence of the sheet resistance of the sample capped with 2 nm of Al. It shows a metallic behavior from 300 to ~ 1 K [see the supplementary material Fig. S1(a)] and then undergoes a superconducting transition. The orange and blue lines in Fig. 1 correspond to the data measured with the current along $[\bar{1}\bar{1}0]$ and $[\bar{1}\bar{1}2]$ directions, respectively. The difference in the resistance along $[\bar{1}\bar{1}2]$ and $[\bar{1}\bar{1}0]$ directions at low temperatures suggests the presence of a strong in-plane anisotropy as demonstrated by previous studies.³⁶ The sample undergoes a superconducting transition along both directions, with T_c (middle of the transition) ~ 0.82 and 0.58 K. The magnetoresistance and Hall measurements at 2 K were carried out to estimate the carrier density

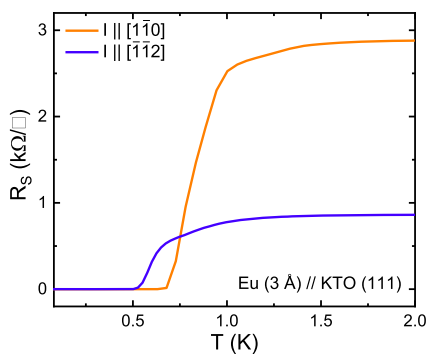


FIG. 1. Transport measurement. Temperature dependence of the sheet resistance measured with current parallel to $[\bar{1}\bar{1}0]$ (orange) and $[\bar{1}\bar{1}2]$ (blue) directions where the superconducting transitions are observed at temperatures $T_c = 0.82$ and 0.58 K, respectively.

and mobility (see the supplementary material for detailed discussion). The mobilities were quite different along $[\bar{1}\bar{1}2]$ and $[\bar{1}\bar{1}0]$, amounting to 111 and 33 $\text{cm}^2 \text{V}^{-1} \text{s}^{-1}$, respectively. This hints at an anisotropy in the band structure between the Γ -M and Γ -K directions.

B. Band structure of Eu/KTO (111) 2DEG

The band dispersion of the Eu(3 Å)/KTO (111) sample was measured along the Γ -K and Γ -M directions with a photon energy of 31 eV at normal emission; see Figs. 2(a) and 2(d). The data clearly indicate an anisotropic electronic structure. By performing a manual photon energy scan, we also found photon emission intensity close to 106 eV of photon energy. This photon energy is similar to the one reported by Bruno *et al.*⁴⁵ However, we found the highest photoemission intensity at 31 eV and, thus, in the following, we show the band structures measured using 31 eV of photon energy. The sample is superconducting, but the ARPES measurements were carried out in the normal state at 15 K. Tight-binding fits of the band structure are overlaid on the ARPES dispersion data. Out of the eighteen pairs of bands in our TB model, four are visible in the measurement window. Similar to our previous report on KTO (001),³⁵ we have associated four different colors for each pair of bands. The pink and green band pairs arise from the t_{2g} orbitals, whereas orange and cyan band pairs are the contribution from another copy of the sub-band arising due to the quantum confinement of the 2DEG. We have also considered the mixing of Ta 5d orbitals and the spin-orbit coupling. In Ref. 35, we could easily identify the orbital character of each band pair. However, unlike in KTO (001) 2DEGs, all three t_{2g} orbitals are highly hybridized in the case of KTO (111) 2DEGs and, therefore, it is not possible to ascribe a specific orbital character to each band pair, as also discussed in Ref. 45. However, the contribution of orbitals with a given character depends on the in-plane direction. This can be inferred from the clear asymmetry observed in the contrast of Fig. 2(d), where the pink band pairs are better visible in the data along the Γ -M' direction, whereas the green band pair is better visible along the Γ -M direction. The energy distribution curves (EDC) at $k = 0$ [Figs. 2(c) and 2(f)] and momentum distribution curves (MDC) at Fermi energy (E_F) [Figs. 2(b) and 2(e)] corresponding to the dispersion curves for both Γ -K and Γ -M directions are analyzed to determine the quality of the TB fits with respect to the experimental observation of the band structure. The detailed analysis is discussed in the supplementary material. Furthermore, the pink band pair in Fig. 2(d) appears to be heavier in the raw data around $k = \pm 0.2 \text{ \AA}^{-1}$ in comparison with the fit. An explanation for the apparent enhancement of the effective mass of the pink band pair could be an electron-phonon interaction that causes parabolic bands to look kinked below a certain binding energy. This effect has been observed previously in STO 2DEGs.⁴⁸ The disagreement between the fit and the data occurs because our model does not consider electron-phonon coupling. From the TB calculation, we can estimate the effective mass. We find that the cyan and green band pairs exhibit a lower effective mass of $0.67 m_e$ at the Γ point in comparison with the orange and pink band pairs, which have a higher effective mass of $1.45 m_e$, where m_e is the electron mass. In general, the effective masses are k -dependent and anisotropic. The Rashba splittings near the Γ point have also been calculated from the TB model. For the pink and orange band pairs, the splitting is isotropic near Γ with

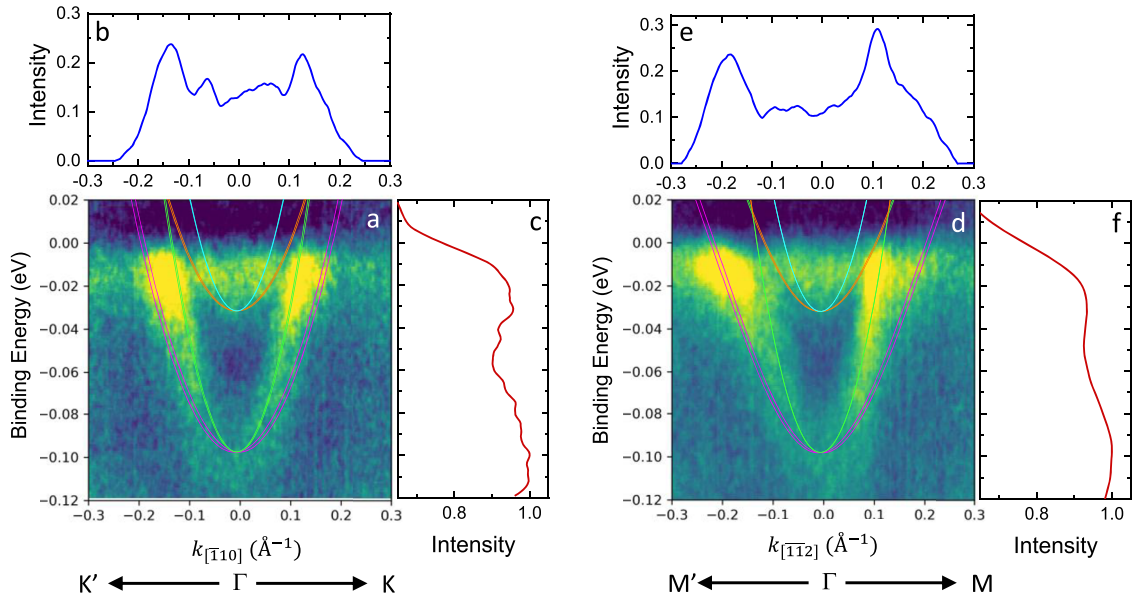


FIG. 2. Electronic band structure of KTO (111) 2DEG. Band dispersion of Eu/KTO (111) 2DEG measured by ARPES along high symmetry directions (a) Γ -K and (d) Γ -M. The tight-binding fits of the band structure are overlaid on the data, where a specific color is associated with each pair of bands. Momentum distribution curves (MDC) at E_F are shown in (b) for Γ -K and in (e) for Γ -M directions. Energy distribution curves (EDC) at Γ are shown in (c) and (f).

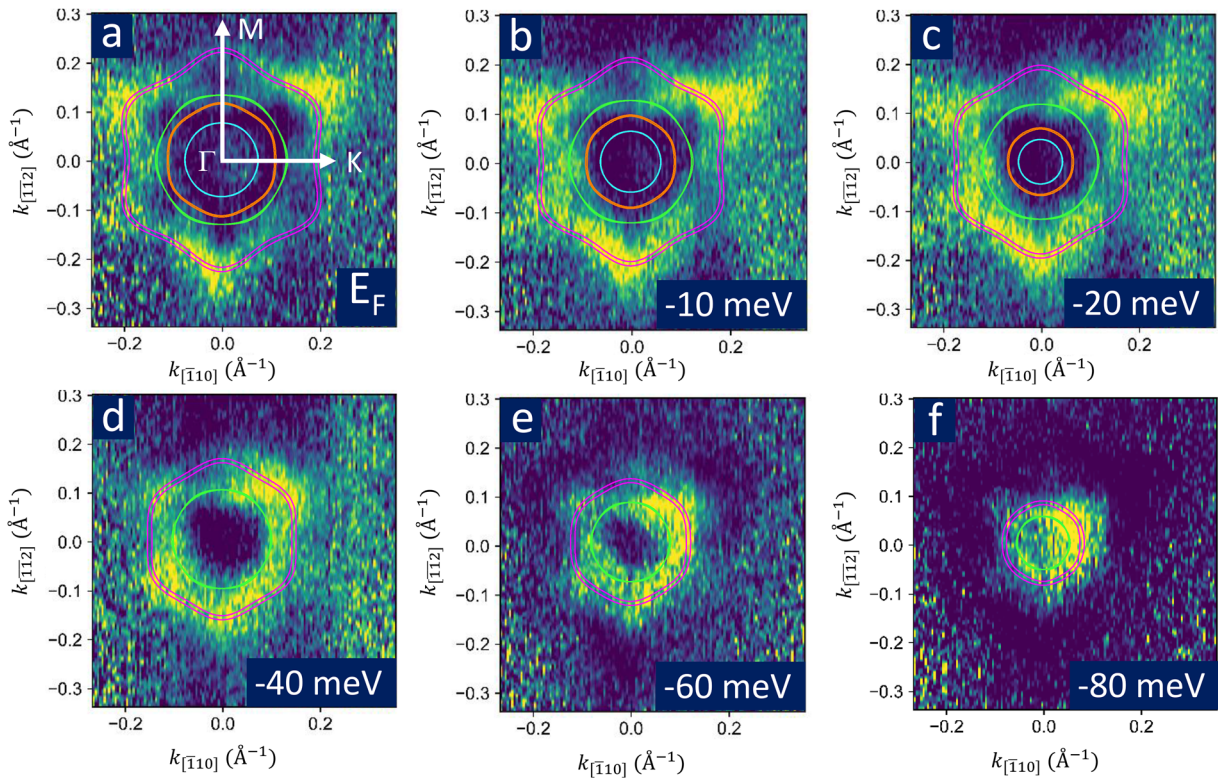


FIG. 3. Fermi surfaces. Constant energy maps with their corresponding tight-binding fit at (a) Fermi energy (E_F) and (b) 10 meV, (c) 20 meV, (d) 40 meV, (e) 60 meV, and (f) 80 meV below the Fermi level. The high symmetry points (Γ , M, and K) and their directions are shown with white arrows in (a).

07 March 2024 11:53:45

values of $\alpha_R = 20$ and 8 meV \AA^{-1} , respectively. For the green and cyan bands, the splitting is anisotropic. It is zero along Γ -M and has values of $\alpha_R = 14$ and 4 meV \AA^{-1} along Γ -K, respectively. The α_R values obtained for KTO (111) 2DEGs are comparatively smaller with respect to the high α_R of $\sim 300 \text{ meV \AA}^{-1}$ observed for the heavy band pair in KTO (001) 2DEGs.³⁵ A similar reduction in α_R was observed in the case of the SrTiO₃ (111)-based 2DEGs in comparison with the (001)-based ones.⁴⁹ We have not performed photon energy scans to prove the two-dimensional nature of the Eu/KTO (111) electron gas. However, from the dispersion measurements, we observe sub-bands that are indicative of quantum confinement and consistent with a 2DEG.

Figure 3 shows constant energy maps and their corresponding TB fits for different binding energies. We observe a star-shaped Fermi surface centered at Γ with three concentric FSs. The star-shaped FS fitted by the pink band pair displays a major diameter of $\sim 0.47 \text{ \AA}^{-1}$ along the Γ -M direction and a minor diameter of $\sim 0.35 \text{ \AA}^{-1}$ along the Γ -K direction. Although the general star shape of the outermost FS matches the one reported by Bruno *et al.*,⁴⁵ the ratio between the major and minor diameters differs, suggesting a slightly different shape of the FS in the case of an MBE-grown KTO (111) based 2DEG compared to a free KTO (111) surface. At $E_F = 0$, the TB fits suggest star-shaped FSs for the pink and orange band pairs, whereas the green and cyan band pairs display hexagonal and circular-shaped FSs, respectively. The total carrier density

calculated from the TB model is $12.5 \times 10^{13} \text{ cm}^{-2}$. This is in good agreement with the carrier density ($11.4 \times 10^{13} \text{ cm}^{-2}$) obtained from the first transport measurements performed just after the ARPES measurements (see the supplementary material for a detailed discussion). Bruno *et al.* discussed in their TB model that each branch of the outermost star-shaped FS can possess different orbital characteristics.⁴⁵ Our measurements [Figs. 3(a)–3(c)] with LH polarization reveal the branches having d_{xz} and d_{xy} orbital characteristics and limit the possibility of visualizing the branches possessing d_{yz} orbital characteristics, which is consistent with Ref. 45.

C. Spin textures of the fitted bands

To understand the spin texture of the 2DEG, we have extended the TB calculation to compute the spin textures for all band pairs at different iso-energy lines. The spin textures for all the band diagrams shown in Fig. 3 are depicted in Fig. 4. The size and direction of the arrows correspond to the magnitude and in-plane orientations of the spins. The color of the arrows indicates the out-of-plane component, with red along $[111]$ and blue along $[\bar{1}\bar{1}\bar{1}]$. In our previous study of KTO (001) 2DEGs, we showed that near the band edge, each band pair has a k-linear Rashba-like splitting with almost circular iso-energy lines and perpendicular spin-momentum locking.³⁵ On the contrary, for KTO (111) 2DEGs, the spin textures exhibit perpendicular spin-momentum locking only at the pink and orange band

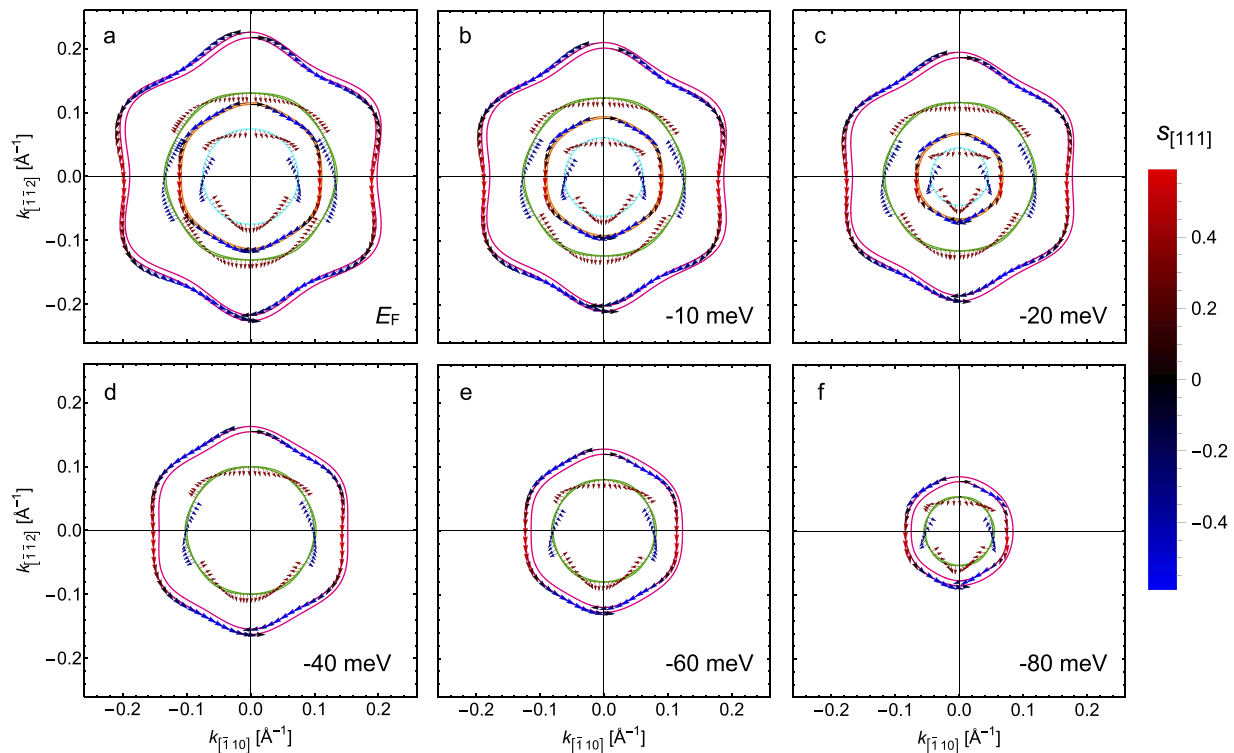


FIG. 4. Spin textures. The fitted iso-energy lines from Fig. 3 (same colors), with arrows indicating the spin texture. The arrow orientation and size correspond to the in-plane component. Their color indicates the out-of-plane component, with red along $[111]$ and blue along $[\bar{1}\bar{1}\bar{1}]$. In each panel, the left (right) half shows the spins of the outer (inner) band of each band pair. The spins of the green and cyan bands reverse at some points of the Fermi lines as the inner and outer bands intersect.

pairs along the high symmetry directions, i.e., along Γ -K and Γ -M. The surface of KTO (111) has C_{3v} symmetry with the mirror planes perpendicular to $(1\bar{1}0)$, which is reflected in the iso-energy lines as well as the spin textures shown in Fig. 4. The C_{3v} symmetry forces the states at each mirror plane (states along Γ -M and equivalent directions) to have a zero spin component parallel to the mirror plane. Hence, the spin texture is in-plane at the tips of the star-shaped pink band pair but exhibits sizable out-of-plane components in between. Furthermore, the momentum splitting for each pair of sub-bands is not the same at every k point. As previously determined in Ref. 45, the splitting for the pink and green band pairs is larger along the Γ -K direction than along the Γ -M direction. From the ARPES data, we observe that the bands of neighboring band pairs are closer along the Γ -K direction, which gives rise to a situation of avoided crossing similar to that found in the STO (001) band structure.²¹ Therefore, the momentum splitting as well as the Rashba coupling constant is greater close to these points. This should motivate experiments to study the Edelstein effect in such systems. The C_{3v} symmetry of the system allows an in-plane spin polarization perpendicular to an in-plane applied charge current. However, the magnitude of the spin polarization as well as its orientation with respect to the charge current does not depend on the direction of the applied charge current. Despite the nonzero out-of-plane components of the spin texture, the net current-induced spin polarization is expected to be in-plane, enforced by the C_{3v} symmetry of the system.

IV. CONCLUSION

In summary, we have visualized the electronic band structure of superconducting KTO (111) 2DEGs using ARPES. The results show similarities with those reported on KTO (111) surfaces, with the following main features: (i) the Fermi surfaces of the bands from the outer pair have a pronounced anisotropic, star-like shape, while the other bands have more isotropic Fermi surfaces (inside the measurement window); (ii) the spin textures strongly deviate from a standard Rashba model, showing considerable warping for the outer band pair and radial rather than orthoradial spins for some of the inner bands; and (iii) the band splitting is moderate at the band bottoms but larger at the end of and in between the branches of the star. The anisotropy of the Fermi surfaces and spin textures echo that of the superconducting critical temperature and mobility, and our results thus constrain the applicability of the models proposed to explain superconductivity in KTO 2DEGs.⁴² The in-plane anisotropy of the system suggests that spin-charge conversion effects from the Rashba-Edelstein effect should be highly anisotropic and deviate from predictions using standard models,¹⁷ which could bring novel functionalities for spin-orbitronics.

SUPPLEMENTARY MATERIAL

The supplementary material contains information regarding the transport measurement, x-ray photoelectric spectra (XPS) and low energy electron diffraction (LEED) for the substrate as well as the sample, the analysis related to energy distribution curves (EDC) and momentum distribution curves (MDC), and additional ARPES data measured using linear vertical (LV) polarization.

ACKNOWLEDGMENTS

This work was supported by the ANR QUANTOP Project (No. ANR-19-CE470006) and the ERC Advanced grant “FRESCO” (Grant No. 833973). I.M. acknowledges the support from the DFG under SFB TRR 227.

AUTHOR DECLARATIONS

Conflict of Interest

The authors have no conflicts to disclose.

Author Contributions

S.M., B.G., and H.W. contributed equally to this paper.

Srijani Mallik: Conceptualization (equal); Investigation (lead); Writing – original draft (lead). **Börge Göbel:** Methodology (lead); Writing – original draft (equal). **Hugo Witt:** Investigation (supporting); Writing – original draft (equal). **Luis M. Vicente-Arche:** Investigation (equal); Writing – original draft (supporting). **Sara Varotto:** Investigation (equal). **Julien Bréhin:** Investigation (supporting); Writing – review & editing (supporting). **Gerbold Ménard:** Investigation (supporting). **Guilhem Saïz:** Investigation (supporting). **Dyhia Tamsaout:** Investigation (supporting). **Andrés Felipe Santander-Syro:** Investigation (supporting). **Franck Fortuna:** Investigation (supporting). **François Bertran:** Investigation (supporting). **Patrick Le Fèvre:** Investigation (supporting). **Julien Rault:** Investigation (supporting). **Isabella Boventer:** Writing – review & editing (supporting). **Ingrid Mertig:** Funding acquisition (equal); Methodology (equal); Writing – review & editing (supporting). **Agnès Barthélémy:** Investigation (supporting). **Nicolas Bergeal:** Investigation (supporting); Writing – review & editing (supporting). **Annika Johansson:** Conceptualization (equal); Methodology (equal); Writing – review & editing (equal). **Manuel Bibes:** Conceptualization (lead); Funding acquisition (lead); Project administration (lead); Writing – review & editing (equal).

DATA AVAILABILITY

The data that support the findings of this study are available from the corresponding author upon reasonable request.

REFERENCES

- H. Y. Hwang, Y. Iwasa, M. Kawasaki, B. Keimer, N. Nagaosa, and Y. Tokura, “Emergent phenomena at oxide interfaces,” *Nat. Mater.* **11**, 103–113 (2012).
- F. Trier, P. Noël, J.-V. Kim, J.-P. Attané, L. Vila, and M. Bibes, “Oxide spin-orbitronics: Spin-charge interconversion and topological spin textures,” *Nat. Rev. Mater.* **7**, 258–274 (2022).
- A. Ohtomo and H. Y. Hwang, “A high-mobility electron gas at the $\text{LaAlO}_3/\text{SrTiO}_3$ heterointerface,” *Nature* **427**, 423–426 (2004).
- T. C. Rödel, F. Fortuna, S. Sengupta, E. Frantzeskakis, P. L. Fèvre, F. Bertran, B. Mercey, S. Matzen, G. Agnus, T. Maroutian, P. Lecoeur, and A. F. Santander-Syro, “Universal fabrication of 2D electron systems in functional oxides,” *Adv. Mater.* **28**, 1976–1980 (2016).
- L. M. Vicente-Arche, S. Mallik, M. Cosset-Cheneau, P. Noël, D. C. Vaz, F. Trier, T. A. Gosavi, C.-C. Lin, D. E. Nikonov, I. A. Young, A. Sander, A. Barthélémy,

- J.-P. Attané, L. Vila, and M. Bibes, “Metal/SrTiO₃ two-dimensional electron gases for spin-to-charge conversion,” *Phys. Rev. Mater.* **5**, 064005 (2021).
- ⁶C. Grezes, A. Kandazoglou, M. Cosset-Cheneau, L. M. V. Arche, P. Noël, P. Sgarro, S. Auffret, K. Garello, M. Bibes, L. Vila, and J.-P. Attané, “Non-volatile electric control of spin-orbit torques in an oxide two-dimensional electron gas,” *Nat. Commun.* **14**, 2590 (2023).
- ⁷H. P. R. Frederikse, W. R. Thurber, and W. R. Hosler, “Electronic transport in strontium titanate,” *Phys. Rev.* **134**, A442–A445 (1964).
- ⁸J. F. Schooley, W. R. Hosler, and M. L. Cohen, “Superconductivity in semiconducting SrTiO₃,” *Phys. Rev. Lett.* **12**, 474–475 (1964).
- ⁹Y. Z. Chen, N. Bovet, F. Trier, D. V. Christensen, F. M. Qu, N. H. Andersen, T. Kasama, W. Zhang, R. Giraud, J. Dufouleur, T. S. Jespersen, J. R. Sun, A. Smith, J. Nygård, L. Lu, B. Büchner, B. G. Shen, S. Linderoth, and N. Pryds, “A high-mobility two-dimensional electron gas at the spinel/perovskite interface of γ -Al₂O₃/SrTiO₃,” *Nat. Commun.* **4**, 1371 (2013).
- ¹⁰N. Reyren, S. Thiel, A. D. Caviglia, L. F. Kourkoutis, G. Hammerl, C. Richter, C. W. Schneider, T. Kopp *et al.*, “Superconducting interfaces between insulating oxides,” *Science* **317**, 1196–1199 (2007).
- ¹¹A. D. Caviglia, S. Gariglio, N. Reyren, D. Jaccard, T. Schneider, M. Gabay, S. Thiel, G. Hammerl, J. Mannhart, and J.-M. Triscone, “Electric field control of the LaAlO₃/SrTiO₃ interface ground state,” *Nature* **456**, 624–627 (2008).
- ¹²A. D. Caviglia, M. Gabay, S. Gariglio, N. Reyren, C. Cancellieri, and J.-M. Triscone, “Tunable Rashba spin-orbit interaction at oxide interfaces,” *Phys. Rev. Lett.* **104**, 126803 (2010).
- ¹³F. Trier, G. E. Prawiroatmodjo, Z. Zhong, D. V. Christensen, M. von Soosten, A. Bhowmik, J. M. G. Lastra, Y. Chen, T. S. Jespersen, and N. Pryds, “Quantization of Hall resistance at the metallic interface between an oxide insulator and SrTiO₃,” *Phys. Rev. Lett.* **117**, 096804 (2016).
- ¹⁴A. F. Santander-Syro, O. Copie, T. Kondo, F. Fortuna, S. Pailhès, R. Weht, X. G. Qiu, F. Bertran, A. Nicolaou, A. Taleb-Ibrahimi, P. Le Fèvre, G. Herranz, M. Bibes, N. Reyren, Y. Apertet, P. Lecoeur, A. Barthélémy, and M. J. Rozenberg, “Two-dimensional electron gas with universal subbands at the surface of SrTiO₃,” *Nature* **469**, 189–193 (2011).
- ¹⁵G. Berner, M. Sing, H. Fujiwara, A. Yasui, Y. Saitoh, A. Yamasaki, Y. Nishitani, A. Sekiyama, N. Pavlenko, T. Kopp, C. Richter, J. Mannhart, S. Suga, and R. Claessen, “Direct *k*-space mapping of the electronic structure in an oxide-oxide interface,” *Phys. Rev. Lett.* **110**, 247601 (2013).
- ¹⁶S. McKeown Walker, S. Riccò, F. Y. Bruno, A. de la Torre, A. Tamai, E. Golias, A. Varykhalov, D. Marchenko, M. Hoesch, M. S. Bahrany, P. D. C. King, J. Sánchez-Barriga, and F. Baumberger, “Absence of giant spin splitting in the two-dimensional electron liquid at the surface of SrTiO₃ (001),” *Phys. Rev. B* **93**, 245143 (2016).
- ¹⁷D. C. Vaz, F. Trier, A. Dyrdał, A. Johansson, K. Garcia, A. Barthélémy, I. Mertig, J. Barnaś, A. Fert, and M. Bibes, “Determining the Rashba parameter from the bilinear magnetoresistance response in a two-dimensional electron gas,” *Phys. Rev. Mater.* **4**, 071001 (2020).
- ¹⁸L. F. Mattheiss, “Energy bands for KNiF₃, SrTiO₃, KMoO₃, and KTaO₃,” *Phys. Rev. B* **6**, 4718–4740 (1972).
- ¹⁹E. Lesne, Y. Fu, S. Oyarzun, J. C. Rojas-Sánchez, D. C. Vaz, H. Naganuma, G. Sicoli *et al.*, “Highly efficient and tunable spin-to-charge conversion through Rashba coupling at oxide interfaces,” *Nat. Mater.* **15**, 1261 (2016).
- ²⁰J.-Y. Chauléau, M. Boselli, S. Gariglio, R. Weil, G. de Loubens, J.-M. Triscone, and M. Viret, “Efficient spin-to-charge conversion in the 2D electron liquid at the LAO/STO interface,” *Europhys. Lett.* **116**, 17006 (2016).
- ²¹D. C. Vaz, P. Noël, A. Johansson, B. Göbel, F. Y. Bruno, G. Singh, S. McKeown-Walker, F. Trier, L. M. Vicente-Arche, A. Sander, S. Valencia, P. Bruneel, M. Vivek, M. Gabay, N. Bergeal, F. Baumberger, H. Okuno, A. Barthélémy, A. Fert, L. Vila, I. Mertig, J.-P. Attané, and M. Bibes, “Mapping spin-charge conversion to the band structure in a topological oxide two-dimensional electron gas,” *Nat. Mater.* **18**, 1187–1193 (2019).
- ²²S. Ohya, D. Araki, L. D. Anh, S. Kaneta, M. Seki, H. Tabata, and M. Tanaka, “Efficient intrinsic spin-to-charge current conversion in an all-epitaxial single-crystal perovskite-oxide heterostructure of La_{0.67}Sr_{0.33}MnO₃/LaAlO₃/SrTiO₃,” *Phys. Rev. Res.* **2**, 012014 (2020).
- ²³T. Rödel, C. Baille, F. Fortuna, C. Baumier, F. Bertran, P. Le Fèvre, M. Gabay, O. Hijano Cubelos, M. Rozenberg, T. Maroutian, P. Lecoeur, and A. Santander-Syro, “Orientational tuning of the Fermi sea of confined electrons at the SrTiO₃ (110) and (111) surfaces,” *Phys. Rev. Appl.* **1**, 051002 (2014).
- ²⁴S. McKeown Walker, A. De La Torre, F. Bruno, A. Tamai, T. Kim, M. Hoesch, M. Shi, M. Bahrany, P. King, and F. Baumberger, “Control of a two-dimensional electron gas on SrTiO₃ (111) by atomic oxygen,” *Phys. Rev. Lett.* **113**, 177601 (2014).
- ²⁵G. Singh, A. Jouan, G. Herranz, M. Scigaj, F. Sánchez, L. Benfatto, S. Caprara, M. Grilli, G. Saiz, F. Couëdo, C. Feuillet-Palma, J. Lesueur, and N. Bergeal, “Gap suppression at a Lifshitz transition in a multi-condensate superconductor,” *Nat. Mater.* **18**, 948–954 (2019).
- ²⁶A. Jouan, S. Hurand, G. Singh, E. Lesne, A. Barthélémy, M. Bibes, C. Ulysse, G. Saiz, C. Feuillet-Palma, J. Lesueur, and N. Bergeal, “Multiband effects in the superconducting phase diagram of oxide interfaces,” *Adv. Mater. Interfaces* **9**, 2201392 (2022).
- ²⁷S. H. Wemple, “Some transport properties of oxygen-deficient single-crystal potassium tantalate (KTaO₃),” *Phys. Rev.* **137**, A1575–A1582 (1965).
- ²⁸P. D. C. King, R. H. He, T. Eknapakul, P. Buaphet, S.-K. Mo, Y. Kaneko, S. Harashima, Y. Hikita, M. S. Bahrany, C. Bell, Z. Hussain, Y. Tokura, Z.-X. Shen, H. Y. Hwang, F. Baumberger, and W. Meevasana, “Subband structure of a two-dimensional electron gas formed at the polar surface of the strong spin-orbit perovskite KTaO₃,” *Phys. Rev. Lett.* **108**, 117602 (2012).
- ²⁹A. F. Santander-Syro, C. Baille, F. Fortuna, O. Copie, M. Gabay, F. Bertran, A. Taleb-Ibrahimi, P. Le Fèvre, G. Herranz, N. Reyren, M. Bibes, A. Barthélémy, P. Lecoeur, J. Guevara, and M. J. Rozenberg, “Orbital symmetry reconstruction and strong mass renormalization in the two-dimensional electron gas at the surface of KTaO₃,” *Phys. Rev. B* **86**, 121107 (2012).
- ³⁰K. Zou, S. Ismail-Beigi, K. Kisslinger, X. Shen, D. Su, F. J. Walker, and C. H. Ahn, “LaTiO₃/KTaO₃ interfaces: A new two-dimensional electron gas system,” *APL Mater.* **3**, 036104 (2015).
- ³¹A. Gupta, H. Silitia, A. Kumari, M. Dumen, S. Goyal, R. Tomar, N. Wadehra, P. Ayyub, and S. Chakraverty, “KTaO₃—The new kid on the spintronics block,” *Adv. Mater.* **34**, 2106481 (2022).
- ³²K. Ueno, S. Nakamura, H. Shimotani, H. T. Yuan, N. Kimura, T. Nojima, H. Aoki, Y. Iwasa, and M. Kawasaki, “Discovery of superconductivity in KTaO₃ by electrostatic carrier doping,” *Nat. Nanotechnol.* **6**, 408–412 (2011).
- ³³J. R. Thompson, L. A. Boatner, and J. O. Thomson, “Very low-temperature search for superconductivity in semiconducting KTaO₃,” *J. Low Temp. Phys.* **47**, 467–475 (1982).
- ³⁴L. M. Vicente-Arche, J. Bréhin, S. Varotto, M. Cosset-Cheneau, S. Mallik, R. Salazar, P. Noël, D. C. Vaz, F. Trier, S. Bhattacharya, A. Sander, P. Le Fèvre, F. Bertran, G. Saiz, G. Ménard, N. Bergeal, A. Barthélémy, H. Li, C. Lin, D. E. Nikonov, I. A. Young, J. E. Rault, L. Vila, J. Attané, and M. Bibes, “Spin-charge interconversion in KTaO₃ 2D electron gases,” *Adv. Mater.* **33**, 2102102 (2021).
- ³⁵S. Varotto, A. Johansson, B. Göbel, L. M. Vicente-Arche, S. Mallik, J. Bréhin, R. Salazar, F. Bertran, P. L. Fèvre, N. Bergeal, J. Rault, I. Mertig, and M. Bibes, “Direct visualization of Rashba-split bands and spin/orbital-charge interconversion at KTaO₃ interfaces,” *Nat. Commun.* **13**, 6165 (2022).
- ³⁶C. Liu, X. Yan, D. Jin, Y. Ma, H.-W. Hsiao, Y. Lin, T. M. Bretz-Sullivan, X. Zhou, J. Pearson, B. Fisher, J. S. Jiang, W. Han, J.-M. Zuo, J. Wen, D. D. Fong, J. Sun, H. Zhou, and A. Bhattacharya, “Two-dimensional superconductivity and anisotropic transport at KTaO₃ (111) interfaces,” *Science* **371**, 716–721 (2021).
- ³⁷S. Mallik, G. C. Ménard, G. Saiz, H. Witt, J. Lesueur, A. Gloter, L. Benfatto, M. Bibes, and N. Bergeal, “Superfluid stiffness of a KTaO₃-based two-dimensional electron gas,” *Nat. Commun.* **13**, 4625 (2022).
- ³⁸E. G. Arnault, A. H. Al-Tawhid, S. Salmani-Rezaie, D. A. Muller, D. P. Kumah, M. S. Bahrany, G. Finkelstein, and K. Ahadi, “Anisotropic superconductivity at KTaO₃ (111) interfaces,” *Sci. Adv.* **9**, eadf1414 (2023).
- ³⁹W. Qiao, Y. Ma, J. Yan, W. Xing, Y. Yao, R. Cai, B. Li, R. Xiong, X. C. Xie, X. Lin, and W. Han, “Gate tunability of the superconducting state at the EuO/KTaO₃ (111) interface,” *Phys. Rev. B* **104**, 184505 (2021).

- ⁴⁰X. Hua, F. Meng, Z. Huang, Z. Li, S. Wang, B. Ge, Z. Xiang, and X. Chen, “Tunable two-dimensional superconductivity and spin-orbit coupling at the EuO/KTaO₃(110) interface,” *npj Quantum Mater.* **7**, 97 (2022).
- ⁴¹M. N. Gastiasoro, M. E. Temperini, P. Barone, and J. Lorenzana, “Theory of superconductivity mediated by Rashba coupling in incipient ferroelectrics,” *Phys. Rev. B* **105**, 224503 (2022).
- ⁴²C. Liu, X. Zhou, D. Hong, B. Fisher, H. Zheng, J. Pearson, J. S. Jiang, D. Jin, M. R. Norman, and A. Bhattacharya, “Tunable superconductivity and its origin at KTaO₃ interfaces,” *Nat. Commun.* **14**, 951 (2023).
- ⁴³T. Esswein and N. A. Spaldin, “First-principles calculation of electron-phonon coupling in doped KTaO₃,” [arXiv:2210.14113](https://arxiv.org/abs/2210.14113) [Cond-Mat.mtrl-Sci] (2023).
- ⁴⁴C. Bareille, F. Fortuna, T. C. Rödel, F. Bertran, M. Gabay, O. H. Cubelos, A. Taleb-Ibrahimi, P. Le Fèvre, M. Bibes, A. Barthélémy, T. Maroutian, P. Lecoeur, M. J. Rozenberg, and A. F. Santander-Syro, “Two-dimensional electron gas with six-fold symmetry at the (111) surface of KTaO₃,” *Sci. Rep.* **4**, 3586 (2014).
- ⁴⁵F. Y. Bruno, S. McKeown Walker, S. Riccò, A. de la Torre, Z. Wang, A. Tamai, T. K. Kim, M. Hoesch, M. S. Bahramy, and F. Baumberger, “Band structure and spin-orbital texture of the (111)-KTaO₃ 2D electron gas,” *Adv. Electron. Mater.* **5**, 1800860 (2019).
- ⁴⁶E. A. Martinez, J. Dai, M. Tallarida, N. M. Nemes, and F. Y. Bruno, “Anisotropic electronic structure of the 2D electron gas at the AlO_x/KTaO₃(110) interface,” *Adv. Electron. Mater.* **9**, 2300267 (2023).
- ⁴⁷X. Chen, T. Yu, Y. Liu, Y. Sun, M. Lei, N. Guo, Y. Fan, X. Sun, M. Zhang, F. Alarab, V. N. Stokov, Y. Wang, T. Zhou, X. Liu, F. Lu, W. Liu, Y. Xie, R. Peng, H. Xu, and D. Feng, “Orientation-dependent electron-phonon coupling in interfacial superconductors LaAlO₃/KTaO₃,” [arXiv:2301.13488](https://arxiv.org/abs/2301.13488) [cond-mat.supr-con] (2023).
- ⁴⁸P. D. C. King, S. McKeown Walker, A. Tamai, A. de la Torre, T. Eknapakul, P. Buaphet, S.-K. Mo, W. Meevasana, M. S. Bahramy, and F. Baumberger, “Quasiparticle dynamics and spin-orbital texture of the SrTiO₃ two-dimensional electron gas,” *Nat. Commun.* **5**, 3414 (2014).
- ⁴⁹P. K. Rout, E. Maniv, and Y. Dagan, “Link between the superconducting dome and spin-orbit interaction in the (111) LaAlO₃/SrTiO₃ interface,” *Phys. Rev. Lett.* **119**, 237002 (2017).